VIP Organic Light-Emitting Diodes

DOI: 10.1002/anie.201206289

Enhanced Electroluminescence Efficiency in a Spiro-Acridine Derivative through Thermally Activated Delayed Fluorescence**

*Gábor Méhes, Hiroko Nomura, Qisheng Zhang, Tetsuya Nakagawa, and Chihaya Adachi**

Organic light-emitting diodes (OLEDs) are expected to find use in large-scale consumer electronics applications, including general illumination and displays, because of their advantages over current technologies in terms of luminescent properties, power consumption, and shape and size variability.[1] The quantum-statistical branching ratio of the electron–hole pairs under electrical excitation means that the internal quantum efficiency (η_{int}) of fluorescent OLEDs is limited to 25%, whereas phosphorescent OLEDs can achieve an η_{int} value of 100%, because both singlet and triplet excitons can be harvested.[2] Although phosphorescent OLEDs have reached their η_{int} limit,[3] they have some disadvantages, including lower electroluminescence efficiency under high current densities[4] and rather low reliability in the blue region of the visible spectrum for practical applications. To overcome these problems, alternative exciton formation processes have been explored. Thermally activated delayed fluorescence (TADF, E-type delayed fluorescence) is a promising way to obtain a high efficiency of exciton formation by converting spin-forbidden triplet excitons up to the singlet level by the mechanism of reverse intersystem crossing (RISC). In a TADF emitter, the upconversion mechanism uses the vibronic energy that, at sufficiently high temperatures ($\geq$ 300 K), allows all of the excitons in an OLED to eventually produce light through singlet decay.[5,6,12]

Although TADF is a well-known phenomenon, it was not applied in OLEDs until recently, because TADF materials typically exhibit low internal photoluminescence (PL) efficiency (η_{PL}).[6] In 2009, we demonstrated for the first time that electrically activated TADF from a tin(IV) fluoride–octaethylporphine complex (SnF_2OEP) gradually increased the exciton generation efficiency over the measured range of temperatures from 300 K to 400 K.[5] High external quantum efficiencies (η_{ext}) of more than 10% have already been reported for OLEDs containing copper complexes.[7,8] However, unlike pure organic molecules, Cu complexes show limited molecular design possibilities and have rather low morphological and electrochemical stabilities.[9] In 2011, we designed an organic molecule containing indolocarbazole and triazine moieties as the electron donor and acceptor units, respectively; this molecule showed a TADF efficiency that was almost ten times higher than that of SnF_2OEP.[6] A device containing this organic compound showed a TADF component of 29% out of the total η_{PL} of 39%, exceeding the theoretical η_{ext} limit for fluorescent OLEDs. To date, there are few examples of OLEDs using TADF and even fewer involve purely organic compounds.

In this study, we demonstrate efficient TADF activated by a spiro-acridine derivative at room temperature with high η_{PL} values (more than 67%) for the first time, thereby confirming that TADF can prevail over conventional fluorescence. The PL characteristics of a pure film of the spiro-acridine compound and of a doped film are presented, and an efficient TADF-based OLED with a maximum η_{ext} value of 10% is realized, thus surpassing the physical limitations of devices that contain only a fluorescent emitter (assuming outcoupling efficiency of 20%). Exceptionally strong quenching of the delayed fluorescence by atmospheric oxygen was observed in a solid-state film, thereby allowing the TADF contribution to PL in an oxygen-free environment to be clearly demonstrated. We believe that organic molecules that are composed of aromatic units and show highly efficient TADF will become the ideal choice for OLED emitters.

A small energy difference between the lowest singlet (S_1) and lowest triplet (T_1) excited states (ΔE_{ST}) is needed to realize efficient TADF.[10] According to Boltzmann statistics, the smaller the ΔE_{ST} value at a given temperature, the easier it is to achieve RISC.[11] In other words, a small ΔE_{ST} value means that there is a small overlap integral between the wave functions of the ground and excited states of a luminescent molecule, thus minimizing electron–electron repulsion between the electron orbitals in the triplet state.[5] In this context, the ground state of the molecule is equivalent to the highest occupied molecular orbital (HOMO) level, and the excited state is in turn equivalent to the lowest unoccupied molecular orbital (LUMO) level. One useful strategy to minimize the overlap between the wave functions is to localize the electron densities of the HOMO and LUMO states on donor and acceptor moieties, respectively.[6] Additional steric separation that is achieved by introducing a spiro junction or bulky substituents between the acceptor and donor units also helps this effect.[6] Based on the former idea, we recently used TADF in a spirobifluorene derivative to produce an OLED with $\eta_{ext} = 4.4\%$, despite its rather low η_{PL} value of 27%.[12]

[*] G. Méhes, H. Nomura, Dr. Q. Zhang, Dr. T. Nakagawa, Prof. Dr. C. Adachi
Department of Applied Chemistry
Center for Organic Photonics and Electronics Research
Kyushu University
744 Motooka, Nishi, Fukuoka 819-0395 (Japan)
E-mail: adachi@opera.kyushu-u.ac.jp
Homepage: http://www.cstf.kyushu-u.ac.jp/~adachilab/

[**] This research was funded by the Japan Society for the Promotion of Science (JSPS) through the "Funding Program for World-Leading Innovative R&D on Science and Technology (FIRST Program)," initiated by the Council for Science and Technology Policy (CSTP).

Supporting information for this article is available on the WWW under http://dx.doi.org/10.1002/anie.201206289.

We followed the design considerations outlined above and synthesized a donor–acceptor structure consisting of an acridine donor that is spiro-conjugated in the C-9 position of a fluorene unit. Two CN groups were attached to the fluorene moiety to enhance its electron-accepting ability. The structure of the resulting molecule, 10-phenyl-10H-spiro[acridine-9,9′-fluorene]-2′,7′-dicarbonitrile (ACRFLCN), is shown in Figure 1a. The electron density of the LUMO state is localized on the nitrile-functionalized fluorene

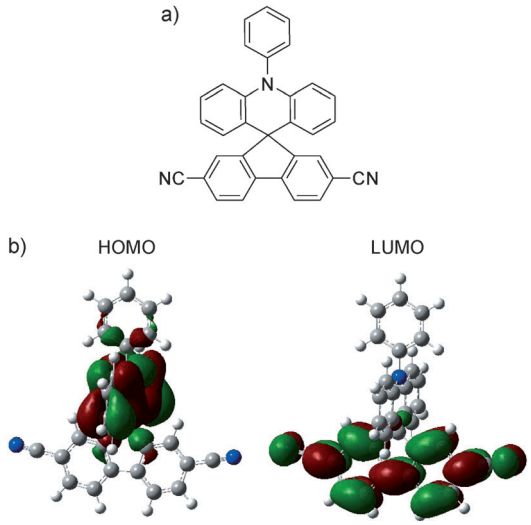

Figure 1. a) Molecular structure of ACRFLCN. b) Electron density distributions in the HOMO and LUMO states calculated by TD-DFT in Gaussian 09 at the B3LYP/6-31G(d) level. Blue N, gray C, white H. Green: positive, red: negative isosurfaces of molecular orbitals.

acceptor, while that of the HOMO state is localized on the acridine donor, as predicted by time-dependent density functional theory (TD-DFT) calculations in Gaussian 09 (Figure 1b). ΔE_{ST} was calculated to be just 0.0083 eV, thus suggesting potentially high RISC.

Upon UV excitation, a pure ACRFLCN film exhibited a broad greenish-yellow emission centered around 530 nm with a large Stokes shift of approximately 100 nm (Figure 2; all experiments presented herein were carried out at room temperature, unless otherwise stated). The characteristic unstructured band with a full width at half maximum (FWHM) of almost 100 nm is assumed to be the result of charge transfer (CT) between the donor and acceptor units. Bearing in mind that this material is intended for use as an emitter in OLEDs, its absolute η_{PL} value of 5.5% was definitely considered to be low. To avoid self-quenching, ACRFLCN was then doped into a triphenyl-[4-(9-phenyl-9*H*-fluoren-9-yl)phenyl]silane (TPSi-F)[13] host, which has a wide energy gap (Figure S1 in the Supporting Information). Host layers must possess a higher T_1 energy than the guest to prevent backward energy transfer from the guest to the host. All further analyses were performed using a codeposited film containing 6 wt% ACRFLCN in TPSi-F. T_1 levels were derived from the phosphorescence peaks of a pure TPSi-F film (2.74 eV) and an ACRFLCN film (2.50 eV) at low temperatures (36 K and 11.5 K, respectively).

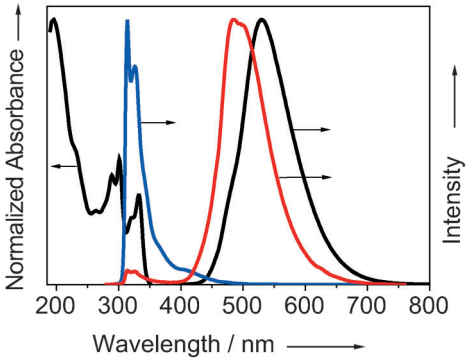

Figure 2. Absorption and fluorescence spectra of a neat ACRFLCN film (black); fluorescence spectra of a TPSi-F neat film (blue) and a co-deposited film containing 6 wt% ACRFLCN in TPSi-F (red). The arrows indicate which y-axis belongs to a certain trace.

The PL emission spectrum of the codeposited film showed a CT emission peak at 485 nm, which was blue-shifted compared to the peak of pure ACRFLCN, and another low-intensity peak around 315 nm originating from the host; this peak was not observed in the spectrum of ACRFLCN (Figure 2). The η_{PL} value of the codeposited film measured in air at atmospheric pressure (10.7%) was almost twice as high as that of the pure film (5.5%). In contrast, a relatively high η_{PL} value of approximately 67% was observed for a 6 wt% ACRFLCN:TPSi-F codeposited film in a nitrogen-rich environment (Figure 4). The large difference between these efficiency values allows TADF to be clearly demonstrated simply by flowing nitrogen gas over a sample in air under UV irradiation (see Figure 3a,b, and the video file in the Supporting Information).

To gain better insight into the photophysical processes leading to the highly efficient PL of the 6 wt% doped film, we measured the transient PL using a streak camera both in air and under vacuum (ca. 3 Pa). As shown in Figure 4, the PL exhibits second-order exponential decay in air, where the delayed component (assigned to weak TADF) decays completely within approximately 4 ms (the decay constant of the delayed component is $\tau_{del} \approx 0.41$ ms; see Table S2 in the Supporting Information). In contrast, under vacuum, the delayed component's contribution increased significantly (the emission spectrum is embedded in Figure 4). In fact, even after around 40 ms, a low-intensity peak corresponding to the main peak of the guest could still be resolved ($\tau_{del} = 3.9$ ms; see Table S2 in the Supporting Information). The sensitivity of the emission to oxygen and the presence of the delayed component with the long emission decay time in the fluorescence spectral region are typical of TADF. In the latter case, the best fitting was achieved by using a third-order exponential decay model. The contributions of the prompt and delayed (TADF) components to the efficiencies are listed in Table 1 (the method used to determine these values is detailed in the Supporting Information). In air, the TADF component makes a larger contribution than the fluorescence (Φ_{rel_F} and Φ_{rel_TADF}, the relative efficiencies of the fluorescence and the TADF to η_{PL}, respectively, have a ratio of 0.36:0.64), thus giving η_{PL} values of fluorescence (Φ_F) and

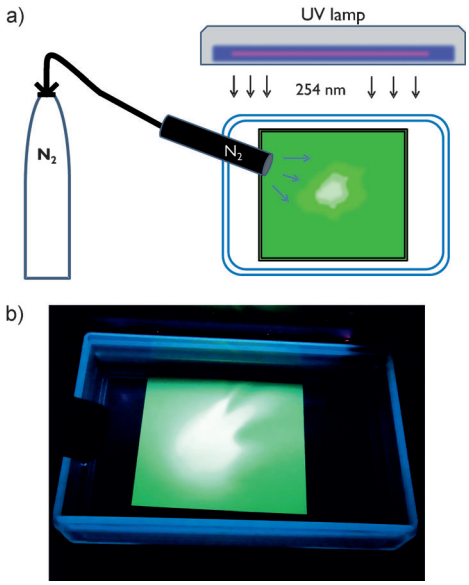

Figure 3. Nitrogen flow experiment. a) Schematic diagram of experimental setup, and b) photograph demonstrating enhanced TADF in a codeposited film (6 wt% ACRFLCN:TPSi-F) on a 45 mm^2 Si substrate by temporarily removing oxygen from the film surface by directing a nitrogen gas flow over the sample under constant UV irradiation (254 nm). See also video file in the Supporting Information.

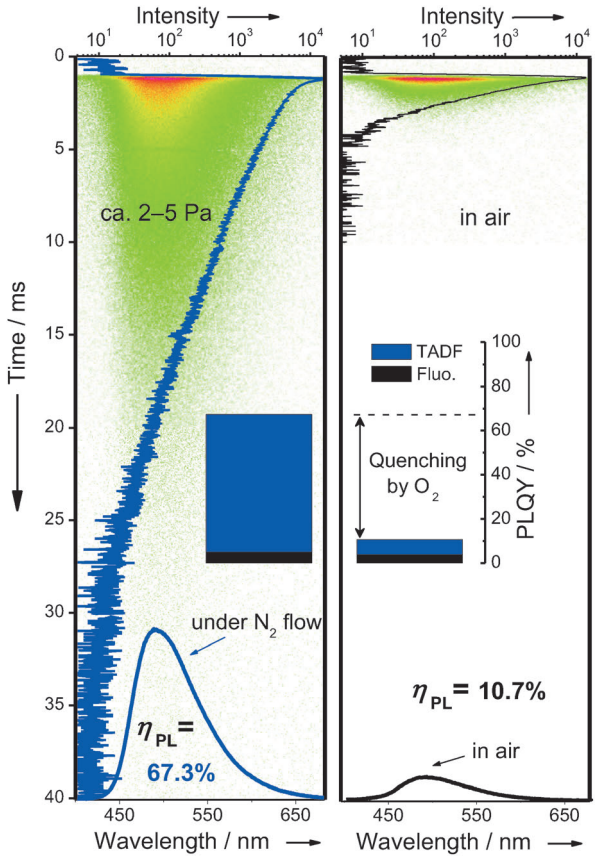

Figure 4. Transient PL decay curves for a codeposited film measured using a streak camera in air at atmospheric pressure (black) and a vacuum of approximately 3 Pa (blue); the curves are integrated into the streak images by matching the time and spectral axes (the number of green dots is proportional to the photon count; coloring towards red indicates higher photon counts). Embedded at the bottom are the PL spectra that were measured by using a spectrometer with an integrating sphere at constant absorption before (black) and after (blue) the elimination of oxygen from the equipment by nitrogen gas saturation. The same setup was used to measure η_{PL} for corresponding events. Owing to limitation of the experimental setup, vacuuming was not possible in the latter case; nevertheless saturation by nitrogen is considered to be equal in excluding oxygen quenching. The embedded rectangular diagrams represent combined results from transient decays and η_{PL} showing the relative contributions from fluorescence and TADF to the overall emission. PLQY = PL quantum yield.

TADF (Φ_{TADF}) of 3.86% and 6.84%, respectively. Under vacuum, while the η_{PL} value of the prompt component had a somewhat higher value of 4.87%, the delayed emission had a very high efficiency of $\Phi_{TADF} = 62.43\%$, thus meaning that $\Phi_{rel\_F}/\Phi_{rel\_TADF} = 0.07{:}0.93$.

The TADF enhancement mechanism under vacuum or in a nitrogen-rich environment is described in Figure 5. Excitation of a sample to higher singlet levels, S_n, is followed by internal conversion (IC) to the S_1 level (2.68 eV). From this point, while some of the energy relaxes through low-efficiency fluorescence (around 7% of the total emission), most of the excitons decay to the T_1 state (2.58 eV) by intersystem crossing (ISC). This process is followed by thermal upconversion to the S_1 state (RISC), thereby leading to TADF. Because the thermal recycling process between T_1 and S_1 continues for a relatively long time (> ms), in air it leads to efficient nonradiative deactivation by energy exchange with the environmental oxygen. However, when oxygen is removed from the system by evacuation or by the nitrogen flow, very efficient RISC from the T_1 to the S_1 levels leads to an intense delayed emission (comprising 93% of the total emission). The experimental value for ΔE_{ST} was estimated from the fluorescence and phosphorescence spectra of the codeposited film (Figure 6). The streak data measured at room temperature over a time span of 10 ms showed that the prompt and delayed spectra overlapped completely, which is characteristic of TADF, and the low-temperature phosphorescence spectrum was slightly red-shifted in comparison to the prompt and delayed spectra at room temperature. To prove the thermal activation of TADF, we monitored the PL emission in a temperature range from 5 K to 325 K and estimated the temperature-dependent values for η_{PL} and for prompt and delayed emission (Figure S3 in the Supporting Information). The upconversion through TADF starts around 100 K, and a complete spectral transformation from the characteristic ππ* shape of phosphorescence to the CT* shape of delayed fluorescence occurs around 200 K. From the

Table 1: PL efficiencies of a 6 wt% ACRFLCN:TPSi-F film and electroluminescence (EL) efficiencies of the OLED device.

Conditions	η_{PL} [%]	Φ_F [%]	Φ_{TADF} [%]	Φ_{rel_F}	Φ_{rel_TADF}	η_{theo} [%]	η_{ext} [%]
Atmospheric	10.7	3.86	6.84	0.36	0.64	0.25	–
Oxygen-free	67.3	4.87	62.43	0.07	0.93	12.7	10.1

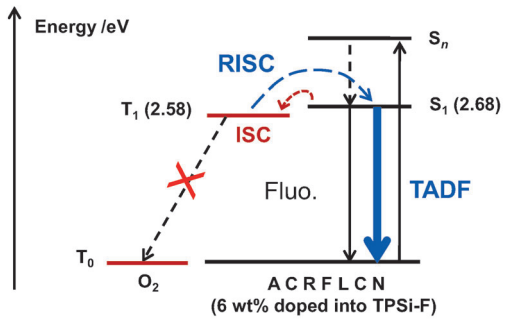

Figure 5. Modified Jablonski diagram explaining enhanced TADF by elimination of oxygen quenching.

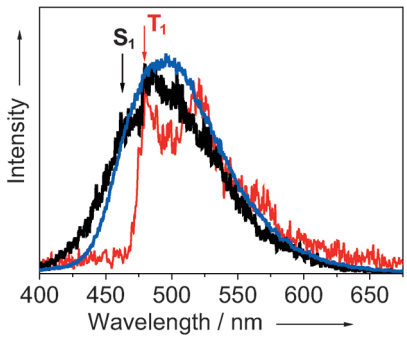

Figure 6. PL emission spectra of codeposited film recorded with a streak camera. Fluorescence (black) and TADF (blue) spectra were recorded at room temperature using <0.25 ms and >0.5 ms time windows of a 10 ms time range, respectively. The phosphorescence (red) spectrum was measured at 10 K, by using a time range of 10 ms and omitting the prompt fluorescence.

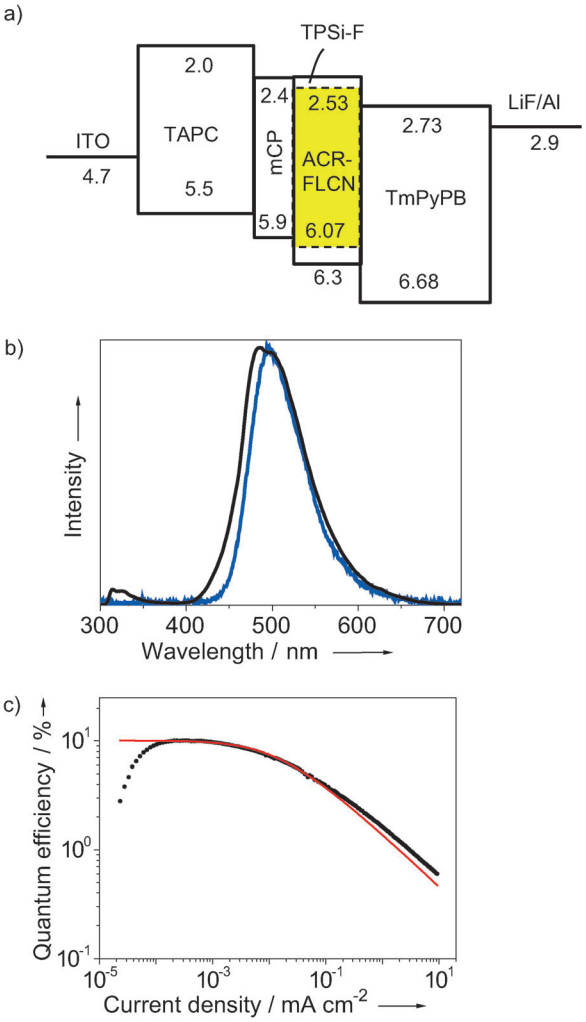

Figure 7. a) Energy diagram of organic materials used in the prototype OLED. The energy values are all given in eV. b) PL (black) and EL (blue; at 10 mA cm^{-2}) spectra measured from this OLED. c) External quantum efficiency (η_{ext}) determined from the current density characteristics of this device. The red line in (c) represents the fitting of the TTA model.[16]

spectra shown in Figure 6, the value of ΔE_{ST} was experimentally determined to be 0.10 eV. Because of the difficulty in determining the S_1 level exactly from the PL spectrum, we also calculated ΔE_{ST} using the Berberan–Santos method[19] (Figure S4 in the Supporting Information) and obtained a value of 0.028 eV, which is much closer to that of the theoretical prediction of 0.0083 eV. From the same analysis, we determined the ISC yield (Φ_T) to be a very high value of 96.4%. In accordance with the Φ_T value, the ISC rate constant (k_{isc}) was found to be 7.4×10^7 s^{-1} (the k_{isc} determination method can be found in the Supporting Information).

An emissive molecule with a high η_{PL} value of approximately 67% and a large TADF component enables excitons to be generated with high efficiency in OLEDs. A multilayer OLED that was designed to exceed the limitations of the fluorescence-based OLEDs was fabricated. Figure 7a shows the HOMO and LUMO levels of the molecules used in this device. The OLED structure was: indium tin oxide (ITO; 110 nm)/1,1-bis[(di-4-tolylamino)phenyl]cyclohexane (TAPC; 40 nm)/1,3-bis(9-carbazolyl)benzene (mCP; 5 nm)/6 wt% ACRFLCN:TPSi-F (20 nm)/1,3,5-tri(*m*-pyrid-3-yl-phenyl)benzene (TmPyPB; 35 nm)/lithium-fluoride (LiF; 1 nm)/aluminum (Al; 62 nm). We used 6 wt% ACRFLCN:TPSi-F as the emitting layer. TAPC and TmPyPB (T_1 levels of 2.87 eV[14] and 2.78 eV,[15] respectively) served as the hole and electron transport layers, respectively. The thin mCP layer was used as a hole transport layer with a high T_1 level for better carrier balance, and to reduce the potential barrier for holes travelling from the TAPC layer to the emitting layer. The EL spectrum of this device recorded at 10 mA cm^{-2} and assigned to the TADF emitter is almost identical to the PL spectrum of the codeposited film (Figure 7b). The dependence of η_{ext} on the device current density is presented in Figure 7c (black line). The OLED achieved a high η_{ext} of 10.1% at a low current density of 3.3×10^{-4} mA cm^{-2}. This value of η_{ext} approaches the theoretical maximum (η_{theory}), which was calculated to be 12.7% by a method that we reported.[12] Because our device structure was not fully optimized, we expect the value of η_{ext} to increase upon careful device optimization. The value of η_{ext} decreased rapidly with increasing current densities above 10^{-3} mA cm^{-2}; this effect can be ascribed to triplet–triplet annihilation (TTA). The experimental results fitted the theoretical curve for the TTA model (red line in Figure 7c)[16] well. For TADF-

based OLEDs, the larger the contribution from delayed emission, the more the exciton formation is enhanced. In the case of ACRFLCN, the relatively high η_{ext} value at low current densities is clearly a result of thermally harvested triplet excitons, with a high exciton-formation efficiency of 75.0–94.3 %.[17] This high exciton-formation yield is far superior to that of conventional fluorescence-based OLEDs (25 %) and approaches that of the best phosphorescence-based OLEDs (100 %).

In conclusion, we have demonstrated highly efficient TADF from a spiro-acridine derivative with a high η_{PL} value (67.3 %) in the solid state at room temperature. The contribution of the delayed fluorescence significantly exceeded that of the prompt fluorescence. An OLED using this molecule as an emitter achieved a maximum η_{ext} value of 10.1 %, which is twice that of a fluorescence-based OLED with $\eta_{int} = 100\,\%$. Efficient quenching of the delayed fluorescence by atmospheric oxygen was also observed in the solid state. We believe that optimized designs using this molecular backbone will enhance the TADF performance. These inexpensive, organic aromatic compounds with such high PL efficiencies are attractive for applications such as OLEDs and molecular oxygen sensors.[18]

Received: August 6, 2012
Published online: October 8, 2012

Keywords: fluorescence · luminescence · organic light-emitting diodes · spiro compounds

[1] M. C. Gather, A. Köhnen, K. Meerholz, *Adv. Mater.* **2011**, *23*, 233 – 248.
[2] M. A. Baldo, D. F. O'Brien, Y. You, A. Shoustikov, S. Sibley, M. E. Thompson, S. R. Forrest, *Nature* **1998**, *395*, 151 – 154.
[3] C. Adachi, M. A. Baldo, M. E. Thompson, S. R. Forrest, *J. Appl. Phys.* **2001**, *90*, 5048 – 5051.
[4] M. A. Baldo, C. Adachi, S. R. Forrest, *Phys. Rev. B* **2000**, *62*, 10967.
[5] A. Endo, M. Ogasawara, A. Takahashi, D. Yokoyama, Y. Kato, C. Adachi, *Adv. Mater.* **2009**, *21*, 4802 – 4806.
[6] A. Endo, K. Sato, K. Yoshimura, T. Kai, A. Kawada, H. Miyazaki, C. Adachi, *Appl. Phys. Lett.* **2011**, *98*, 083302.
[7] J. C. Deaton, S. C. Switalski, D. Y. Kondakov, R. H. Young, T. D. Pawlik, D. J. Giesen, S. B. Harkins, A. J. M. Miller, S. F. Mickenberg, J. C. Peters, *J. Am. Chem. Soc.* **2010**, *132*, 9499 – 9508.
[8] Q. Zhang, T. Komino, S. Huang, S. Matsunami, K. Goushi, C. Adachi, *Adv. Funct. Mater.* **2012**, *22*, 2327 – 2336.
[9] K. Goushi, K. Yoshida, K. Sato, C. Adachi, *Nat. Photonics* **2012**, *6*, 253 – 258.
[10] a) B. Valeur, *Molecular Fluorescence: Principles and Applications*, Wiley-VCH, Weinheim, **2002**, p. 41; b) C. Baleizão, S. Nagl, S. M. Borisov, M. Schäferling, O. S. Wolfbeis, M. N. Berberan-Santos, *Chem. Eur. J.* **2007**, *13*, 3643 – 3651.
[11] a) F. A. Salazar, A. Fedorov, M. N. Berberan-Santos, *Chem. Phys. Lett.* **1997**, *271*, 361 – 366; b) J. C. Fister, III, D. Rank, J. M. Harris, *Anal. Chem.* **1995**, *67*, 4269 – 4275.
[12] T. Nakagawa, S.-Y. Ku, K.-T. Wong, C. Adachi, *Chem. Commun.* **2012**, *48*, 9580 – 9582.
[13] P.-I. Shih, C.-H. Chien, C.-Y. Chuang, C.-F. Shu, C.-H. Yang, J.-H. Chen, Y. Chi, *J. Mater. Chem.* **2007**, *17*, 1692 – 1698.
[14] T.-Y. Kim, D.-G. Moon, *Trans. Electr. Electron. Mater.* **2011**, *12*, 84 – 87.
[15] S.-J. Su, T. Chiba, T. Takeda, J. Kido, *Adv. Mater.* **2008**, *20*, 2125 – 2130.
[16] C. Adachi, M. A. Baldo, S. R. Forrest, *J. Appl. Phys.* **2000**, *87*, 8049.
[17] Upper and lower limit values of exciton formation efficiency (η_{EX}) are calculated using the theoretical and observed external quantum efficiency ($\eta_{ext} = 12.7\,\%$ and 10.1 %) and PL efficiency ($\eta_{PL} = 67.3\,\%$) with assumption of ideal carrier balance (η_{CA}) and out-coupling efficiency (η_{OUT}); $\eta_{CA} = 100\%$; $\eta_{OUT} = 20\%$. Then $\eta_{EX} = \eta_{ext}/(\eta_{CA}\eta_{PL}\eta_{OUT})$.
[18] S. Nagl, C. Baleizão, S. M. Borisov, M. Schäferling, M. N. Berberan-Santos, O. S. Wolfbeis, *Angew. Chem.* **2007**, *119*, 2368 – 2371; *Angew. Chem. Int. Ed.* **2007**, *46*, 2317 – 2319.
[19] M. N. Berberan-Santos, J. M. M. Garcia, *J. Am. Chem. Soc.* **1996**, *118*, 9391 – 9394.

